EAI Endorsed Transactions on Energy Web Technical Article EAI.EU

Overcoming Weak Grid Challenges: A Combined Approach to VSI Stability with Impedance Adjustment, Control Optimization, and Microgrid Integration

Harendra Pal Singh[1,*], Sourav Bose[2], Anurag K. Swami[1]

[1]Department of Electrical Engineering, College of Technology, GBPUA&T, Pantnagar,263145, Uttarakahnd, India
[2]Department of Electrical Engineering, NIT Srinagar, 246174, Uttarakahnd, India

Abstract

This paper addresses the challenges in Voltage Source Inverter (VSI) systems connected to weak grids, where frequent impedance changes lead to instability and power quality issues. This research studies how changing grid impedance affects current distortion and the stability of a VSI. It proposes the stability analysis of a single loop controller and optimize its settings using various techniques (ZN-method, PSO, GA) to ensure VSI stability and meet current distortion limits (THD compliance), when grid impedance varies. The primary focus revolves around addressing two key challenges: managing impedance variations at the PCC and enhancing the tracking performance of the PI controller. The VSI-based system connected to the weak grid and in standalone mode is simulated on Typhoon HIL, to validate the effectiveness of obtained optimized controller parameters by changing various conditions like, the output power regulation and sudden load change in a standalone distribution network. The MATLAB/SIMULINK with m-files is utilized for the parameters optimization and controller model simulation purposes. This research is important for developing more reliable and resilient power systems, specifically by investigating the transient behaviour of VSI frequency and voltage under sudden changes, to ensure an uninterruptible power supply to critical loads.

Received on 15 04 2024; accepted on 01 02 2025; published on 06 02 2025

Keywords: Controller stability criterion, Heuristic optimization technique, Power quality, Total Harmonic Distortion, Weak grid condition, Impedance-based stability, Standalone microgrid system.

doi:10.4108/ew.5788

Abbreviations

VSI Voltage Source Inverter
VOC Voltage Oriented Control
CCL Current Control Loop
PCC Point of Common Coupling
PLL Phase Locked Loop
THD Total Harmonic Distortion
SCR Short Circuit Ratio
PSO Particle Swarm Optimization
GA Genetic Algorithm
PID Proportional-Integral-Differential
PI Proportional-Integral
DERs Distributed Energy Resources
GCI Grid-Connected Inverter
GFL Grid-Following Inverter
GFM Grid-Forming Inverter
ITAE Integral of Time multiply by Absolute Error
SVPWM Space Vector Pulse Width Modulation
SRF Synchronously Rotating Frame
SF Stationary Frame
IMC Internal Model Control
HIL Hardware in Loop

Nomenclature

V_{inv} Inverter output voltage
i_{inv} Inverter output current
V_g Grid voltage

*Corresponding author. Email: harendrapal.singh07@gmail.com

i_g Grid current
i_c Capacitor current
I_{sc} Short-circuit current
I_L Load current
L_f Inverter side inductance
L_g grid side inductance
R_f Inverter side resistance
R_g grid side resistance
C_f Filter capacitance
R_d Damping resistance
ω Grid frequency
ω_0 System frequency
ω_c Cut-off frequency
f_{res} Resonant frequency
f_{sw} Switching frequency
S Switching space vector
a_L Inductance ratio
ξ Damping factor
T_{ss} Settling time
M_p Maximum peak overshoot

1. Introduction

Grid Connected Inverters (GCIs) are essential for integrating Distributed Energy Resources (DERs) of varying capacities (small < 10kW, medium 10-1000kW, large 1-10MW) into the power grid [1]. International and national standards (e.g., IEEE 1547 [4], IEC 61727 [5], VDE-AR-4105 [6]) provide guidelines for operation, power quality, safety, and abnormal condition responses [2],[3]. These standards are crucial for the reliable and safe integration of DERs, enabling a sustainable energy transition.

For systems below 69kV, IEEE Std. 519 sets limits to ensure power quality at the PCC [9]. It specifies a 5% maximum total harmonic distortion (THD) and individual voltage distortion below 3%. Additionally, it provides guidelines to limit current distortion based on the grid strength [12]. This standard helps to achieve smooth output current and ensures compliance with grid connection requirements.

This research aims to understand VSI design for weak grid operation while complying with power quality standards. While integrating Renewable Energy Sources (RESs) with weak grids using VSIs is crucial but weak grids with high impedance pose challenges for VSIs. These challenges include voltage drops, current distortion, and potential VSI instability. Solutions lie in advanced control strategies and improved VSI design to ensure stable operation, minimize current distortion, and maintain power quality even under fluctuating grid conditions.

1.1. Motivation

Grid-connected inverter stability involves assessing responses to small and large-scale control signal disturbances [34][32]. Small disturbances might not disturb the synchronization of the VSI but could be a cause of harmonics and voltage instability during grid feeding mode [33]. Analyzing small signal stability can be done with eigenvalue-based or impedance-based methods. Phase Lock Loop (PLL) and Current Control Loop (CCL) interaction in these conditions contributes to current distortion and instability [34]. This research investigates these inverter stability issues, especially in weak grids under dynamic conditions. It explores three impedance-based stability approaches for the VSIs: (i). Control strategy adaptation: Adjusting controller behavior based on changing grid impedance [36]. (ii). VSI output impedance adjustment: Modifying the VSI's output impedance to account for parallel connections [36]. (iii). Impedance-aware design: Designing filters and control parameters considering grid impedance variations to prevent instability [54], [37].

While these methods offer solutions for weak grids, the interaction between the grid impedance and the current control loop can still lead to instability. To reduce attenuation and increase damping (Q-factor) in a system, several strategies can be implemented [12, 36, 59]. These include increasing feedback gain, employing active damping techniques such as additional control loops, optimizing filter components like inductors or capacitors, incorporating passive damping elements such as resistors or snubbers, using filter design techniques to attenuate specific frequency components, optimizing control strategies, and considering system layout and configuration [12]. These approaches aim to enhance system stability and performance by mitigating oscillations and improving damping characteristics, thereby ensuring reliable operation.

Microgrids (MGs) require careful stability analysis, particularly in Islanding (IS) mode due to lower inertia and reliance on RESs [58]. Voltage and small-signal stability concerns are similar to traditional systems, but most research focuses on IS mode due to reduced grid influence [53]. Challenges include power sharing, load compensation, and smooth transitions between IS and grid-connected (GC) modes [60].

To prevent blackout conditions during IS operations, avoiding the overloading of inverters is crucial. Effective control strategies are necessary for handling sudden load changes and smooth transitions between current control (i.e., GC) and voltage control (i.e., IS) modes [61]. Inverter control algorithms offer flexibility but can also introduce instability issues [65]. Droop control offers flexible operation in both GC and IS modes, but minor disturbances can occur during mode transitions [62, 64]. Therefore, the effectiveness of DG control unit significantly influences the stability and robustness of an MG. Various control strategies in the literature can be used for DERs in both GC and IS modes.

1.2. Literature review

While GC mode is generally stable due to the grid's dominance, weak grids demand careful controller design for resilience against impedance variations. Low/medium-level VSIs benefit from improved switching control and filter design for quality output current, but these can impact control bandwidth [13],[14]. For optimal performance, the CCL needs high bandwidth and fast dynamic response. Controller gain selection must consider filter design and power-sharing, and parameters should minimize error from anticipated input values [15],[16]. The fundamental principle of current regulation, comparing reference and measured values to modulate switching behavior, remains central to achieving the desired output [17].

The table 1, provides a concise overview of the factors influencing controller tuning and the corresponding solutions for minimizing transient response times.

Various controller tuning methods exist for VSI systems, aiming for stable operation [18],[19]. Traditional methods like Ziegler-Nichols (1942) rely on process characteristics but are inefficient. In contrast, modern techniques like Particle Swarm Optimization (PSO) (1995) offer efficient and accurate parameter determination using a fitness function like ITAE [20],[21],[27],[28]. PSO utilizes a population of random solutions and refines them iteratively. Similar to Genetic Algorithms, PSO operates within boundaries defined by the Routh-Hurwitz criteria for closed-loop stability [29]. Additionally, hardware considerations like Digital Signal Processors (DSPs) and Field Programmable Gate Arrays (FPGAs) with Space Vector Pulse Width Modulation (SVPWM) are crucial for reducing control delays, dead-time, and mitigating output current harmonics, ensuring overall system reliability and performance [30].

Ensuring the stability and reliability of a distribution network requires the design of a robust VSI system with careful consideration of critical factors given in table (1). However, in situations where generation systems are situated in remote areas, the medium-voltage transmission lines may be extended, resulting in a large inductive grid impedance [22]. If the impedance of the grid is relatively high, the grid is categorized as a weak grid. In accordance with IEEE Std. 1204-1997 [23], a grid is typically deemed weak when the Short Circuit Ratio (SCR) is less than three. Weak grids are often encountered in remote or rural areas that rely on lengthy feeder lines for their power supply. Generally, weak grids face voltage dips and power outages. Here, the research addresses this by ensuring stable voltage (mitigating noise & optimizing the settings), improving responsiveness (enhanced control systems), and integrating stabilizing elements. Microgrids provide localized support, while advanced inverters (grid-forming & following) regulate voltage and enable smooth transitions between independent and grid-connected operation. This multi-pronged approach strengthens weak connections for a more reliable electricity flow.

Based on the preceding discussions, we have prepared a comprehensive comparison, as presented in table 2. This table is highlighting the contributions of this paper by contrasting it with various prior works from the literature. It not only aids in gaining a fundamental comprehension of VSI component design and parameter selection but also provides practical insights for real-world validation.

1.3. Contribution

A comprehensive discussion on VSI design and parameter selection for the lower voltage distribution network level is presented in this work. This work addressing two key challenges: managing impedance variations at the PCC and enhancing the tracking performance of the CCL. Furthermore, the designed inverter is tested in various scenarios like, GC and IS mode of operation for stability analysis. Regarding this, the paper shows the validation and main contributions of this work as follows:

1. The research investigates the impact of grid impedance variability on current distortion and VSI stability.
2. It proposes an investigation of a single loop controller stability and optimizing CCL parameters by using different controller tuning techniques such as ZN - method and PSO and GA, ensuring VSI stability and THD compliance under grid impedance uncertainty.
3. To address the impedance variation in the grid, the transmission line parameters and grid short circuit ratios are changed as per the testing requirements. The two methods are employed to enhance inverter stability: (a) changing the output impedance of the VSI by adjusting the grid-side inductance, and (b) optimizing the parameters for filter design and VSI controller.
4. Single inverter operation in GC mode and three VSI based microgrid operation is done to investigate the stability during transient conditions.

This paper delves into plant model-based tuning rules for VSI current controllers. It explores various crucial factors for optimizing gain values under diverse production rates and grid conditions, ultimately enhancing its performance and real-world adaptability.

This paper is described in the following sections: Section 2 details the system description, Section 3

Table 1. Summarizing the factors influencing controller tuning for minimizing transient response times along with their corresponding solutions.

Factors	*Solutions*
Proportional Gain (K_P)	**(i)**- Experiment with different K_P values through simulation or testing. **(ii)**- Utilize Ziegler-Nichols method or trial-and-error tuning.
Integral Gain (K_I)	**(i)**- Adjust K_I to eliminate steady-state error while minimizing overshoot. **(ii)**- Use ITAE criterion or Auto-Tuning method for optimal K_I value.
Derivative Gain (K_D)	**(i)**- Fine-tune K_D to dampen oscillations and reduce settling time. **(ii)**- Employ derivative kick method or pole placement for optimal K_D value.
Bandwidth Limitations	**(i)**- Analyze system's frequency response and adjust bandwidth settings. **(ii)**- Use Bode plots or frequency domain analysis for optimization.
Filtering and Smoothing	**(i)**- Implement low-pass or moving average filters to remove noise. **(ii)**- Experiment with filter cut-off frequencies and orders for noise reduction.
System Dynamics	**(i)**- Develop accurate models of system dynamics using mathematical equations or system identification techniques. **(ii)**- Use models to predict transient behavior.
Control Strategy	**(i)**- Select appropriate control strategy based on system's characteristics. **(ii)**- Consider alternatives like model predictive control or adaptive control.
Gain Scheduling	**(i)**- Implement algorithms for real-time adjustment of controller gains. **(ii)**- Develop dynamic optimization algorithms for optimal transient response.

Table 2. Comparative analysis across various reference sources in the literature.

Items	**References**	**This paper**
Standards and regulations	[1],[2],[3],[4],[9],[12][23]	✓
Different modeling methods	[13],[15],[48]	GFL and GFM based MG modelling
Filter designing	[12],[45],[44],[43],[47]	With minimum energy storage
Different control techniques	[16],[17],[39],[42].[49]	VOC with PI controller, droop control and seamless operating mode transition
Controller tuning techniques	[18],[19]	ZN, PSO and GA implementation
Optimization techniques	[20],[21],[24], [25],[27],[28]	Heuristic approach
Stability analysis	[29],[32],[53]	in GFL and GFM modes
Seamless transition	[56],[57],[59]	unified control technique
Impedance based stability	[22],[34],[33],[36],[37]	✓
Real-world implementation	[30],[32]	with consideration of different conditions

describes filter designing and parameters selection, Section 4 elaborates controller modeling; sensitivity/fitness function, PSO algorithm and real coded based GA implementation, and designed VSIs parallel operation in IS mode Section 5 gives results and discussion of the different scenario analysis, and Section 6 concludes the work done in the paper.

2. System description

In grid-feeding mode, as shown in fig.1, VSI systems act as controlled current sources, injecting current into the utility and closely tracking the PCC voltage, contributing to maintain the power quality of the connected network [13], [15]. Voltage-oriented control is commonly used for synchronization and control purposes [42].

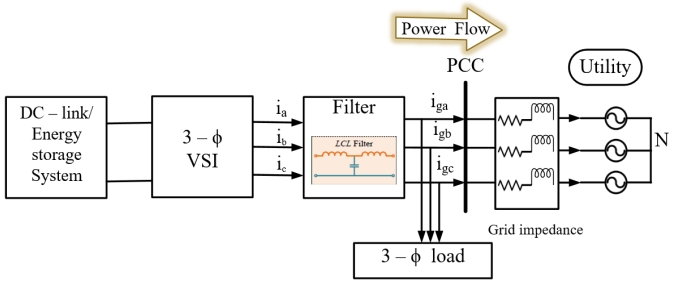

Figure 1. VSI System in Grid Feeding mode.

Regulating the VSI output current effectively controls power delivery to the grid, especially under constant grid voltage, as shown in fig. 2. While power quality

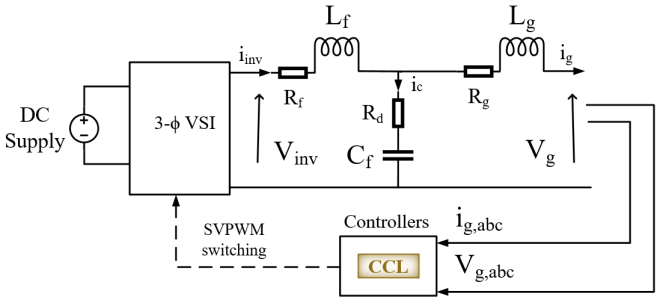

Figure 2. Schematic diagram of grid connected VSI with LCL filter

issues in the PCC voltage can worsen the VSI output current, but appropriate filter design and control parameters can mitigate this effect. This research aims to optimize VSI design parameters for improved system efficiency, reliability, and power quality of output power.

The inverter output voltage and current from fig. 2 can be written as,

$$\begin{bmatrix} V_{inv\_a} \\ V_{inv\_b} \\ V_{inv\_c} \end{bmatrix} = R \begin{bmatrix} i_{g\_a} \\ i_{g\_b} \\ i_{g\_c} \end{bmatrix} + \omega L_T \begin{bmatrix} \frac{di_a}{dt} \\ \frac{di_b}{dt} \\ \frac{di_c}{dt} \end{bmatrix} + \begin{bmatrix} V_{g\_a} \\ V_{g\_b} \\ V_{g\_c} \end{bmatrix} \tag{1a}$$

$$i_{inv\_abc} = i_{c\_abc} + i_{g\_abc} \tag{1b}$$

where $V_{inv_{\{.\}}}$, $i_{inv_{\{.\}}}$, $i_{g_{\{.\}}}$, $i_{\{.\}}$, $i_{c_{\{.\}}}$ and $V_{g_{\{.\}}}$ represents inverter output voltage, inverter output current, grid feeding current, inductor current, capacitor current and the grid voltage of $\{a, b, c\}$ phase respectively. The $R = (R_f + R_g)$, and $L_T = (L_f + L_g)$ where R_f, R_g, L_f and L_g are the inverter side and grid side filter resistance and inductance respectively. R_d is a damping resistor. The C_f is the filter capacitance and ω is the grid frequency.

MGs are defined as controllable groups of DGs units and interconnected loads within specific electrical boundaries, functioning as a single controllable entity concerned with the grid [66],[61]. Unlike traditional distributed systems with significant inertia from large synchronous generators, MGs rely mainly on inverter-based DG systems, offering reduced inertia. In IS mode, micro-sources must fulfill requirements like voltage and frequency control for load sharing. In standalone mode, voltage and current controllers effectively track reference values, assuming ideal inverters. However, this may not true for large size inverters with low switching frequencies. Limited control bandwidth in such cases can lead to transients and deviations from reference values.

3. Filter designing and parameters selection

The filter acts as an intermediary between the VSI and PCC, enhancing the quality of the output current in compliance with IEEE Std.519 guidelines. IEEE Std.519-2022 [10], concerned for harmonic control in electric power systems, which was updated from IEEE Std.519-2014 [11] to include more stringent harmonic limits at the PCC between the utility and the consumers. This is necessary to accommodate the increasing number of non-linear loads on the power system, such as variable frequency drives, and switch-mode power supplies. In GC mode, the proper selection of the filter and power-sharing parameters ensures the power quality within the regulated range and enhances the system performance against the transient conditions. The percentage of current ripple limits and harmonic distortions in output current recommendations are given in table 3, which helps to design the filter components for the VSI-based system.

The higher switching frequency operation inverter applications avoid the use of only inductive components in the filter for the medium and higher power rating inverters because of the bigger size requirement which turns into costly and higher voltage drop across it [45]. Compared to first and second-order filters, the third-order LCL filter has a lower cost and is smaller in size which makes it more suitable for the inverter output connection with the main utility at medium and higher voltage levels. LCL filter provides excellent attenuation of bode 60 dB to the switching frequency. But, in case the grid side impedance is lower, resonance can be triggered, leading to system instability [12]. Moreover, this resonance effect can subsequently cause voltage and current instability in proximity to the resonance frequency. The purpose of applying the resistive damper is to reduce the attenuation and increase the damping (Q - factor) at the characteristic resonance frequency with the minimum power loss. In summary, the design of the LCL filter concerns the following points;

1. Overall filter size, cost, losses
2. Current distortion in different components
3. Resonance and dynamic performance of the overall system
4. Low voltage drop across the filter
5. Higher power factor.

The parameter selection, according to the recommended maximum current distortion limit in the output current set the percentage of current ripples in the inverter output current is the primary concern to describe the lower limits of the filter inductance value. Similarly, the filter capacitance is chosen based on the energy stored in the capacitor. The selection for the filter capacitor is a trade-off between the energy stored in the capacitor and the inverter-side inductance (L_f)

Table 3. Current harmonic limits in the percentage of rated current amplitude according to IEEE 519.

Maximum odd harmonic current distortion in percent of I_L for general distribution system (120 V - 69 kV)						
$\frac{I_{SC}}{I_L}$	$h < 11$	$11 \leq h < 17$	$17 \leq h < 23$	$23 \leq h < 35$	$35 \leq h$	TDD
< 20	4.0	2.0	1.5	0.6	0.3	5.0

*h is the order of harmonics, TDD is Total Demand Distortion

[47]. Increasing the capacitance value results in more reactive power flowing into the capacitor, as well as an increased load current demand from the inverter switches and the L_f (which likely refers to higher conduction and switching losses). While this can help in managing reactive power and stabilizing voltage, it also leads to higher losses and reduced efficiency within the system. Therefore, while higher capacitance can provide benefits in terms of power factor correction and voltage regulation, it comes at the cost of reduced overall system efficiency. The filter inductive reactance should be lower than the capacitive reactance, so the lower the voltage drop across L_f . Generally, the reactive power for the capacitor is chosen between 5 - 15% of the rated capacity as per the requirement.

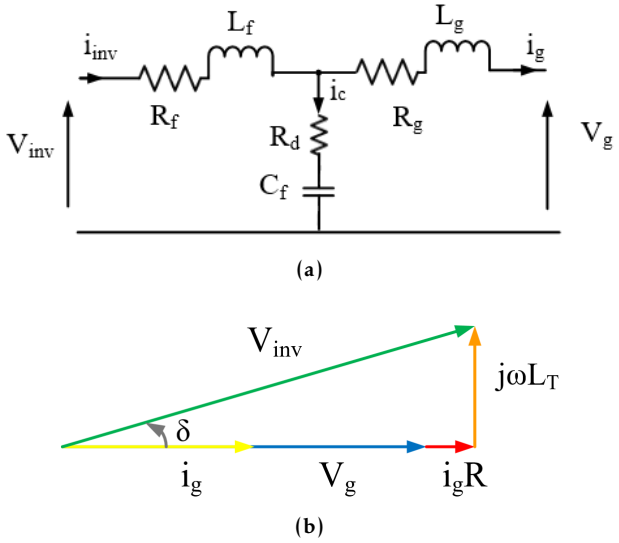

Figure 3. (a).Equivalent circuit diagram of LCL filter connected between VSI and grid, (b). Phasor diagram for the unity power condition.

The following equations represent the circuit shown in fig. 3 (a) and (b). The following equations are used to calculate the transfer function ($G_p(s)$) of the LCL filter:

$$V_{inv} = S\frac{V_{dc}}{2} \tag{2a}$$

$$i_c = i_{inv} - i_g \tag{2b}$$

$$V_{inv} = i_{inv}(R_f + sL_f) + i_c(\frac{1}{sC_f} + R_d) \tag{2c}$$

$$V_g = -i_g(R_g + sL_g) + i_c(\frac{1}{sC_f} + R_d) \tag{2d}$$

where, V_{inv} is the inverter output $3-\phi$ voltage vector, S represents the switching space vector, V_{dc} is the DC - link voltage, i_c is the capacitor current, i_{inv} and i_g are the inverter-side and grid-side currents.

The transfer function of the LCL filter network $G_p(s)$ is considered as a plant for the controllers and calculated from the ratio of output grid current $i_g(s)$ to the inverter output voltage $V_{inv.}(s)$ is represented in eqn. (3);

$$G_p(s) = \frac{i_g(s)}{V_{\text{inv.}}(s)} = \frac{a_1 s + 1}{b_3 s^3 + b_2 s^2 + b_1 s + b_0} \tag{3}$$

where, $a_1 = R_d C_f$, $b_3 = L_f L_g C_f$, $b_2 = C[(L_f + L_g)R_d + L_g R_f + L_f R_g]$, $b_1 = R_d R_g C_f + R_d R_f C_f + R_f R_g C_f + L_f + L_g$, $b_0 = R_f + R_g$. Here, b_3, b_2, b_1 are the grid-side inductance dependent coefficients, which affect the grid connection (stiff/weak grid) requirements.

The resonance frequency of LCL filter is calculated by using eqn. (4) ;

$$f_{\text{res}} = \frac{1}{2\pi}\sqrt{\frac{L_T}{L_f L_g C_f}} \tag{4}$$

Generally, the initial operating conditions of VSI should be determined before selecting the filter parameters, like rated power (P_{rated}), rated i_{inv}, output voltage V_{inv}, inverter switching frequency,f_{sw}, fundamental frequency,f_0. The steps for choosing the LCL filter parameters are as follows:

Step 1. Determine the maximum value for the inverter-side inductance, L_f, based on the maximum value of current ripples in the output current as follows:

$$L_{f\,(max)} = \frac{V_{dc} D}{4 f_{sw} \Delta i|_{max}} \tag{5}$$

where V_{dc} is the input DC voltage, that can obtain from $(2\sqrt{3}(V_{g_{rms}})/M)$, here M is the modulation index,

D is the duty cycle, $\Delta i|_{max}$ is maximum current ripple, that is generally set to be 20 - 30 %. As given in [12], to calculate the minimum inductance value based on switching frequency is given as;

$$L_{f(min)} = \frac{1}{|\omega_{sw} * (\frac{i_{g(sw)}}{V_{i(sw)}}) * (1 - (\frac{\omega_{sw}}{\omega_{res}})^2)|} \tag{6}$$

Step 2. As discussed earlier, determine the filter capacitor value based on the maximum reactive power stored in the capacitor as given below;

$$C_f = 15\% \frac{P_{rated}}{3\omega_0 V_g^2} \tag{7}$$

where P_{rated} is the VSI power rating, ω_0 is fundamental angular frequency.

Step 3. Based on selection of switching frequency, f_{sw}, determine the filter cut-off frequency as $(\frac{1}{10^{th}})$ of (f_{sw}).

Step 4. Determine the minimum inductance value at selected f_{sw} according to the IEEE std. as defined in table II current distortion and harmonic limits, as given in eqn.(6).

Step 5. The maximum and minimum value of inductance provides a selection range for the inverter-side and grid-side inductors to choose the suitable values based on harmonic attenuation and the inductance ratio a_L (i.e., $a_L = \frac{L_f}{L_g}$). The resonance frequency decreases as the grid-side inductance increases with respect to the inverter side. The ratio $a_L = 1$, i.e., $L_f = L_g$, corresponds to the minimum capacitance requirement and lower harmonic attenuation [12].

Step 6. When the THD exceeds 5 %, it is crucial to decrease the attenuation rate to mitigate the distortion and improve power quality. This reduction in the attenuation rate helps in suppressing harmonics more effectively, thereby reducing THD levels and ensuring compliance with quality standards. By decreasing the attenuation rate, the system can better filter out unwanted harmonic frequencies, leading to cleaner power waveforms and enhanced system performance.

Generally, the filter parameters selection includes filtering and controlling issues, which is a trade-off between better filter action (minimum current distortion) and fast dynamic performance. Selected filter parameters are given in the table 4. The trade-off is shown in the results, Section 5.1.1, and minimum current distortion, means better tracking of the reference value.

4. Controller Modelling

In situations where a weak grid connection exists, there is a risk that the controllers may struggle to accurately follow the grid's voltage or angle as a reference, potentially leading to instability in the system. To mitigate this, it is essential to configure the gain values within the CCL according to the characteristics of the plant model to ensure precise tracking performance. Consequently, in order to optimize the performance of Local Control Units (LCUs), it is imperative to meticulously design and fine-tune the control parameters. This is especially critical for maintaining system stability across a wide spectrum of operating conditions, particularly in low voltage distributed networks [32].

This paper utilizing a cascaded two-loop structure (inner and outer) within the Synchronously Rotating Frame (SRF) for VSI system. The inner loop prioritizes minimizing settling times and enhancing dynamic performance during power regulation. It is important to highlight that a single-loop control scheme is typically less robust due to its sensitivity to grid noise (such as harmonics, voltage sags, or transients) while offering a compromise between fast control dynamics and stable steady-state performance [49]. Additionally, filter presence and source inductance can lead to non-unity power factor current, introducing cross-coupling between control axes and limiting the performance. So, decoupling terms are used to cancel out the cross-coupling terms, as shown in fig. 4. To address the reference tracking and system stability challenges, the paper emphasizes the use of single loop control for GCI system which would be crucial for:

1. Mitigating sensitivity to load changes.
2. Enhancing disturbance rejection.
3. Reducing output current THD (especially with non-linear loads).

The controller's role is crucial in maintaining high-quality output current while minimizing THD. Primary controllers with high bandwidth and performance are essential for swift response under diverse operating conditions. They play a pivotal role in coordinating microgrid stability by efficiently managing power distribution among DERs.

As depicted in Fig. 4, it is evident that the voltage and current at the PCC serve as critical references for system operation. However, under weak grid conditions, these measured signals can become distorted. Factors such as low short-circuit ratios, high grid impedance, and system disturbances contribute to voltage and current deviations, making it challenging to maintain accurate signal references for control and stability.. This distortion has an impact on the CCL performance, which needs to be enhanced to improve the overall performance of the VSI. The control problem to be solved here is to determine the controller gain values that ensure the system stability. The purpose of controller tuning is to minimize transient response times, leading to faster system stabilization and more accurate reference tracking. When the

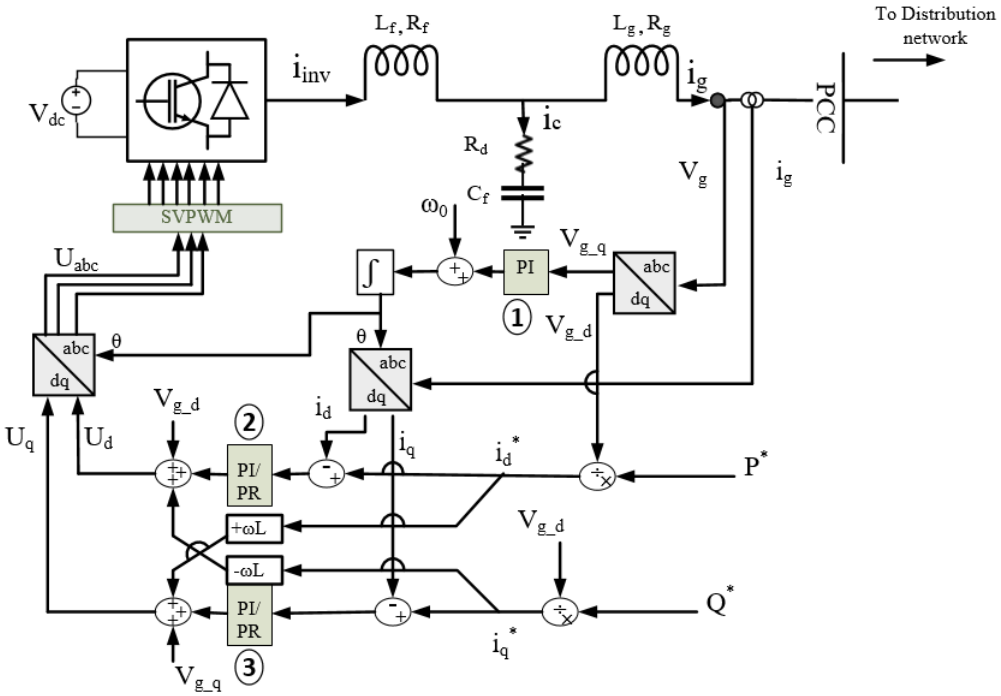

Figure 4. 3ϕ VSI SRF Controller in grid-feeding mode.

parametric uncertainty and performance specifications are specified clearly, controller parameters can be optimized for any possible case.

Problem Formulation

To enhance the stability of a VSI, the controller gain values, filter parameters, and power-sharing parameters must be kept within the prescribed limits. The optimization of controller parameters is synthesized with the offline procedure, ensuring the operating range of the other components. The performance index is based on error (e) minimization and used for further optimization implementation as given in the following equation;

$$\min \int_0^\infty |e(t)|\, dt \quad s.t. K_{P\max} > K_P > K_{P\min}, K_{I\max} > K_I > K_{I\min} \tag{8}$$

Where, $K_{P\max}$ and $K_{P\min}$ are the maximum and minimum values of the proportional gain and $K_{I\max}$ and $K_{I\min}$ are the maximum and minimum values of the integral gain of the PI controller.

4.1. Fitness function

The ITAE performance index criteria to design a control system is derived by using a set of 2^{nd}- order to 8^{th}-order normalized transfer function coefficients to minimize the ITAE index criteria for a step signal [27]. Since it can provide high disturbance rejection capability to the controllers and minimize the overshoot during transients. This index is also often used for small data sets or data obtained from the step response. ITAE performance index trades-off between error magnitude and settling time [50]. In this paper, the fitness function for the controller tuning is based on minimizing the ITAE, which is calculated by using Simpson's 1/3 rule. The expression for the ITAE performance index is given by (9);

$$ITAE = \int_0^\infty t\,|e(t)|\, dt \tag{9}$$

where, t is the time and $e(t)$ is the error produced by the difference between reference and measured value.

4.2. PSO implementation

PSO is an iterative method that depends on the problem searching space to determine the optimal solution for the fitness function shown in Fig. 5. This algorithm is evaluated based on the movement of each particle and the swarm experience. Each particle movement is based on its own experience and collaboration of the swarm. It attracts towards the best local position ($X_{(p,best)}$) experienced by its own and best global position ($X_{(g,best)}$) by the swarm. The basic rules of the PSO algorithm can be briefly described in the following stages; (a). Finding out the fitness value of each particle, (b).Updating the best local and global positions, (c).Updating velocity and best global position

Mathematically, the search process can be represented by the simple equations with concerning

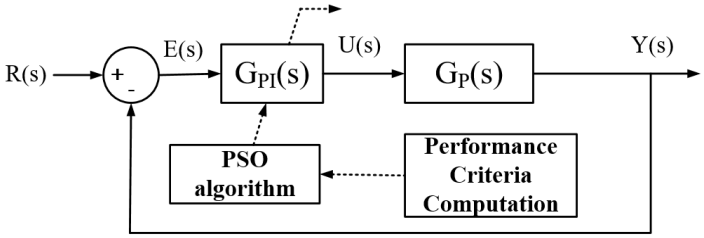

Figure 5. Block diagram of controller tuning using PSO algorithm.

position vector $X_i = (x_{i1}, x_{i2}, \ldots, x_{in})$ and velocity vector $V_i = (v_{i1}, v_{i2}, \ldots, v_{in})$ within the specified selection range. The optimality of the solution depends on each particle's velocity and position which is updated as equation 10 in the algorithm.

$$V_i^{k+1} = w.V_i^k + c_1.r_1[X_{p,best}^k - X_i^k] + c_2.r_2[X_{g,best}^k - X_i^k] \quad (10a)$$

$$X_i^{k+1} = X_i^k + V_i^{k+1} \quad (10b)$$

where, i represents the index of the particle; X_i^k and V_i^k defined as the position and velocity of the particle i at k^{th} iteration, respectively; w represents the inertia weight which can set between [0-1], and also provides the balance between local and global explorations and exploitations which results in fewer iterations on average to find a sufficiently optimal solution; c_1 and c_2 are the acceleration constants used to guide the particle's movement to the p_{best} and g_{best} positions; r_1 and r_2 are the random number variable between [0-1]. PSO algorithm implementation is shown in Fig. 6

Bounded searching space provides fast solutions, but in case the optimum global value is located outside of the boundary conditions, it influences the optimality of the solution [20]. However, the boundary conditions can be extended but this would increase the calculation time and can affect the optimal solution. Therefore, sufficient information about the system parameters limit is beneficial to set the boundary conditions for the search.

4.3. Real coded based GA implementation

The implementation of GA is the same as the PSO algorithm and a search mechanism to find out the optimal solution from the given problems, which is inherently based on its natural selection shown in Fig. 7. GA provides a solution based on the chromosomes that can adapt to the change in the surrounding environmental conditions and are able to reproduce crossover and mutation. In other words, GA simulation is based on the survival of the fittest among individual

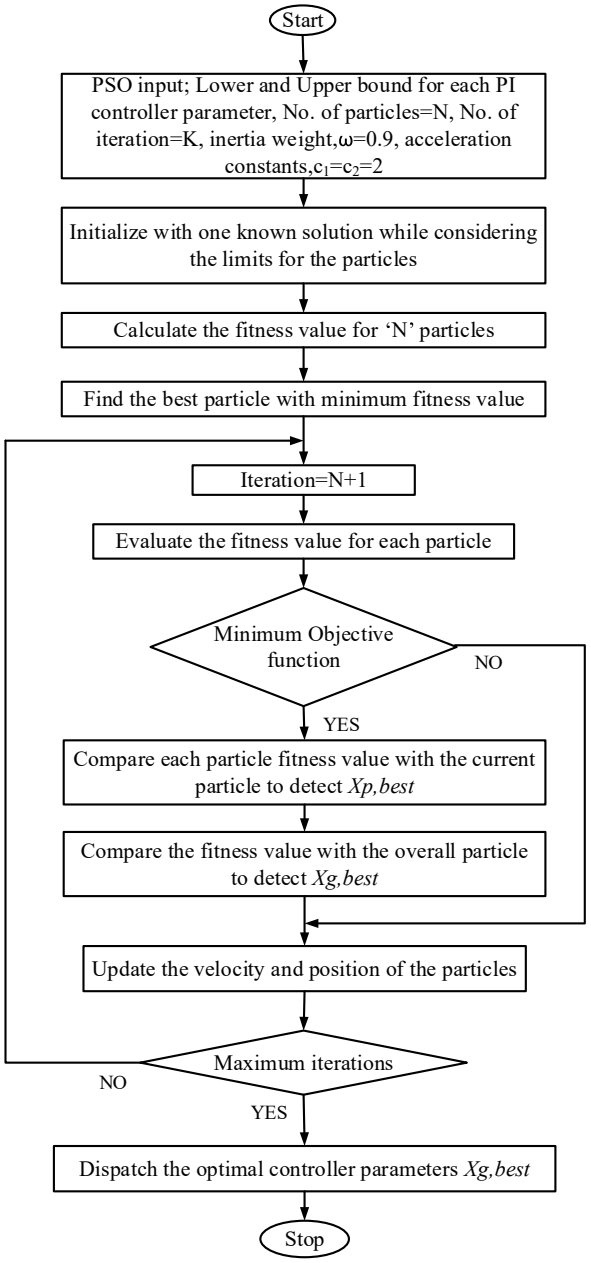

Figure 6. Flowchart of PSO algorithm.

steps of consecutive generations for solving a problem. So, the solution for each successive generation is more adaptable for their search space. The simulated binary crossover (SBX) operator uses a parameter (known as distribution index, η_c) to maintain the positive integer value during the overall running time of the simulation. This parameter has a direct effect on controlling of generation of offspring solutions[26]. The generation of offspring $x_i^{(1,t+1)}$ and $x_i^{(2,t+1)}$ from the parent $x_i^{(1,t)}$ and $x_i^{(2,t)}$ is defined as;

$$\beta_i = \left| \frac{x_i^{(2,t+1)} - x_i^{(1,t+1)}}{x_i^{(2,t)} - x_i^{(1,t)}} \right| \quad (11)$$

where, β_i is called as the spread factor. The probability distribution index is used to create an offspring with similar search power in single point crossover, which can be represented as in (12);

$$\mathcal{P}(\beta_i) = \begin{cases} 0.5(\eta_c + 1)\beta_i^{\eta_c}, & \text{if} \beta_i \leq 1 \\ 0.5(\eta_c + 1)\frac{1}{\beta_i^{\eta_c+2}}, & \text{otherwise} \end{cases} \quad (12)$$

From a defined probability distribution index, the ordinate β_{qi} is found which is helpful for the offspring generation as given in the following eqns.;

$$x_i^{(1,t+1)} = 0.5[(1 + \beta_{q_i})x_i^{(1,t)} + (1 - \beta_{q_i})x_i^{(2,t)}] \quad (13a)$$

$$x_i^{(2,t+1)} = 0.5[(1 - \beta_{q_i})x_i^{(1,t)} + (1 + \beta_{q_i})x_i^{(2,t)}] \quad (13b)$$

Crossover is performed with a higher probability (P_c), whereas the mutation is performed with a low probability (P_m), see Table 4 . If the mutation probability is kept very low, then no element would be mutated by the mutation operator. GA algorithm implementation is shown in Fig. 7

Generally, when the fitness function is provided to GA, it is used to observe the behavior of the function in the given criterion of the problem. So, in the case of the minimization of objective function value, the lowest value would be the most suitable solution for the given situation. The developed algorithm is proposed to find out the optimal controller gain values based on the minimum error.

4.4. GFL modeling

Usually, in GC mode, all DER units employ P-Q control, unless there is a need for ancillary services. The power references (P^* and Q^*) are used to calculate the current reference for the inner control loop. Therefore, the power delivered by the GFL can be directly controlled by the current controller which can be understood by the given formula as follows;

$$p_i = 1.5\,(V_d i_d + V_q i_q) \quad (14a)$$

$$q_i = 1.5\,(V_q i_d - V_d i_q) \quad (14b)$$

The injected current into the grid is ideally in phase with the grid voltage, ensuring unity power factor operation. Consequently, in equations (14a) and (14b), we have $V_q = 0$, which simplifies to $p_i = 1.5 V_d i_d$ and $q_i = -1.5 V_d i_q$. This decoupling enables more effective control of the active and reactive power flow to the grid.

4.5. GFM modeling

In IS mode, inverter-linked DGs act as voltage-controlled sources. To maintain power balance and voltage/frequency stability, they use droop control, mimicking synchronous generator behavior. This control

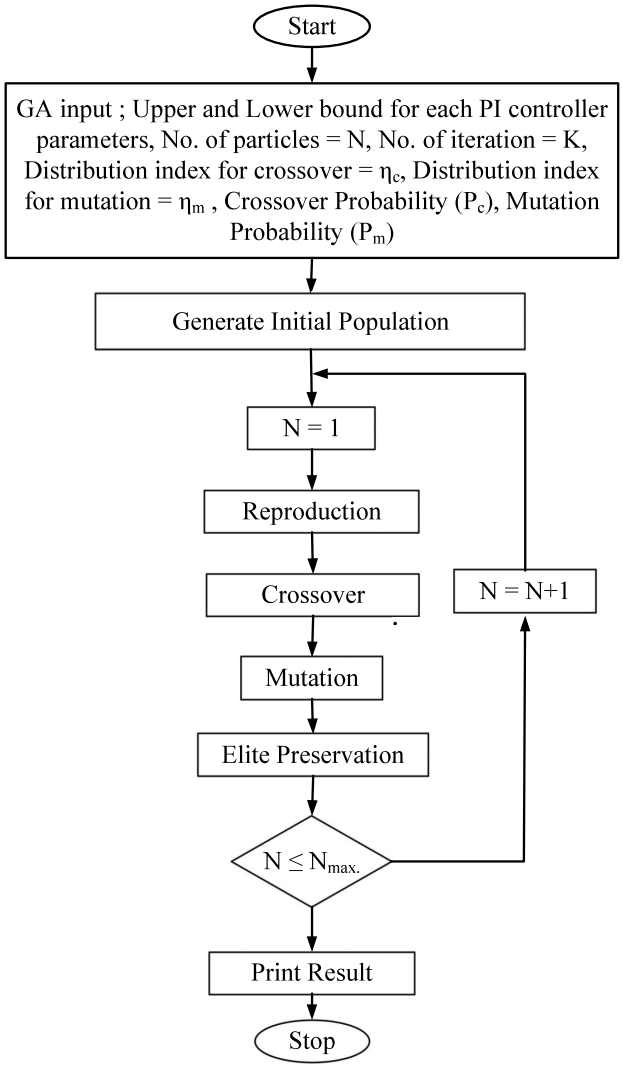

Figure 7. Flowchart of GA algorithm

method sets frequency and voltage amplitude references for each DG based on their active and reactive power output. The equations given in (14a) and (14b) will be passed through the low pass filter to obtain the real and reactive powers P and Q corresponding to the fundamental component.

$$P_i = \frac{\omega_c}{s + \omega_c} p_i \quad (15a)$$

$$Q_i = \frac{\omega_c}{s + \omega_c} q_i \quad (15b)$$

Here, ω_c represents the cut-off frequency of the low pass filter.

As depicted in fig. 4, it is evident that the reference voltage and current are derived from the PCC. When using a single-loop control system in the presence of grid noise, such as fluctuations or disturbances in the electrical grid, the stability of the VSI is compromised. Grid noise can introduce unpredictable variations in the electrical parameters that the control system relies on, leading to instability in the VSI's operation. As a result, the effectiveness of the single-loop control system in regulating the VSI's behavior is limited or constrained. Determining the appropriate controller gain values is critical in control system design. It ensures the system stability while achieving the desired level of tracking performance and meeting the safety and performance requirements. The controller tuning purpose is to minimize the overshoot and time response for transient conditions. When the parametric uncertainty and performance specifications are fixed, controller parameters can be optimized for any possible case.

The finally designed VSI components' parameters are tested under dynamic operating conditions in standalone mode for stability analysis. In standalone mode, three VSI sources are considered to create an isolated microgrid environment with critical and non-critical loads, as shown in fig. 8. The main purpose of this standalone network system is to evaluate the stability and performance of the designed VSI in terms of frequency and voltage stability during the transient condition. It is crucial to investigate any potential disturbance in microgrids, particularly in the islanded mode, because the inertia is low. When operating in the droop control mode, the bus frequency and voltage amplitude reflect, respectively, the output active and reactive power that satisfies the $P-f$ and $Q-V$ droop characteristics. The droop characteristic equations can be expressed as;

$$f = f^{ref} - m(P - P^{ref}) \tag{16a}$$

$$V = V^{ref} - n(Q - Q^{ref}) \tag{16b}$$

where, m and n are the droop coefficients, f^{ref} and V^{ref} are the bus frequency and voltage amplitude at the PCC and P^{ref} and Q^{ref} are the active and reactive power of the DG units.

Overall, droop gain acts as a key control in MG control, influencing power sharing, frequency and voltage regulation, and ultimately, system stability. Selecting appropriate droop gain values based on specific MG conditions is crucial for optimal performance and reliable operation. The heuristic optimization approach could be useful for the parameter's selection during time-domain simulation.

As per the synchronization specifications given in IEEE std 1547.2003 [4], the defined standard range encompasses a voltage magnitude difference ($\triangle V$) within ±10%, a frequency difference of 0.3 Hz, and a phase difference of 20 degrees. The windowing factor-based control logic is described in [56], which is employed to determine the grid's frequency, voltage (V_g) and phase angle. The resynchronization process at PCC involves checking conditions for frequency, voltage amplitude and phase angle fall within desired operating range. If the MG parameters match the grid parameters, the circuit breaker is closed; otherwise, it remains open.

5. Results and Discussion

The proposed GCI system power rating is 10 kW with 3Φ-inductive load, as shown in fig. 1, which is designed and tested in MATLAB/SIMULINK with m-files. The SIMULINK block diagram is given in fig. 4. This paper validates the designed LCL filter for harmonic attenuation and verifies the stability conditions of the controller using the TYPHOON HIL emulator for real-time performance. The controller's design is primarily oriented towards enhancing tracking performance, especially in situations characterized by a less stable grid.

The poles and zeros of the designed filter are in the left half of the s-plane, which represents the filter stability. By additional damping in the filter, the system stability is enhanced, shown in fig 10 (a). As we increase the switching frequency, the filter becomes more effective at eliminating higher-order harmonics. To evaluate stability comprehensively, we have analyzed the gain and phase margins through the plant's transfer function and Bode plots, depicted in fig. 10 (b). This analysis provides insights into the filter's stability and its ability to suppress harmonics, essential for assessing its performance.

A higher switching frequency (refer to table 4) is employed throughout the simulation. This higher frequency assists in the precise tracking of time-varying signals, compensating for dead time, and reducing current ripples in the output current.

The simulation parameters used for the system design are given in table 4.

The selected controller parameters are detailed in both table 4 and table 5. To initiate the optimization processes, the initial parameters for the PSO and GA are derived from the ZN method, which assists in establishing upper and lower limits of the controller gain values. The parameters used in the optimization process are defined in [28, 29] and their values are given in table 4. In fig. 9, a comparative analysis of the PI controller's settling time (T_{ss}) and maximum peak overshoot (M_p) is conducted across different tuning methods, including ZN, PSO, and GA, and the results are summarized in Table 5. Notably, GA outperforms the other methods by achieving optimal best M_p

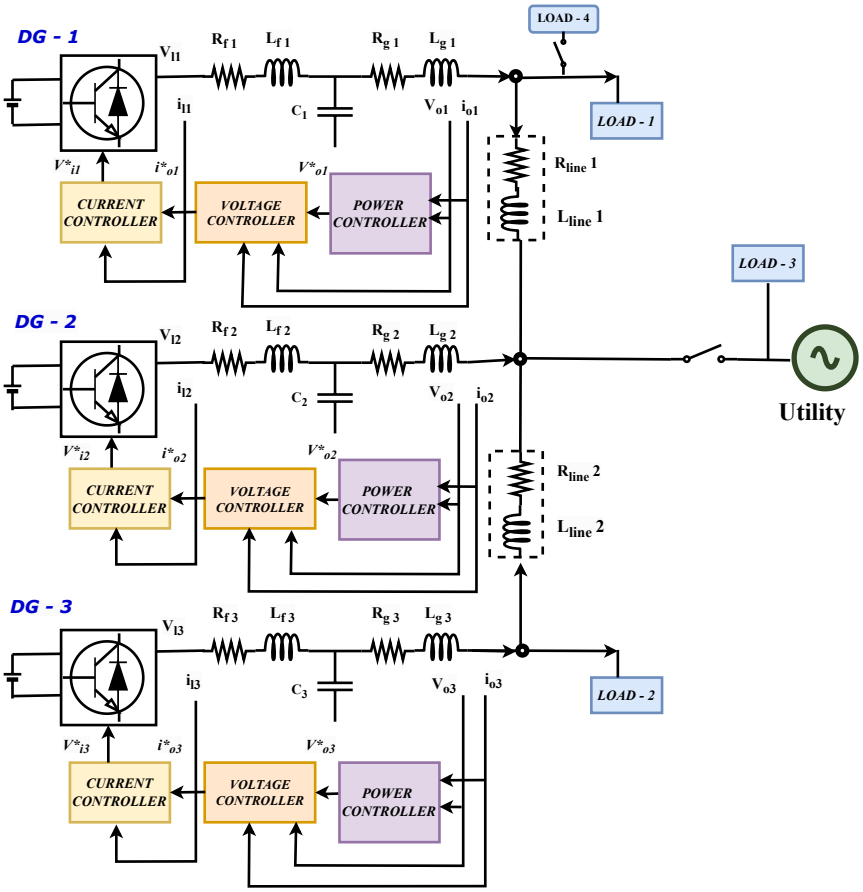

Figure 8. Circuit diagram of three VSI based standalone microgrid system.

Table 4. Selected Parameters for the experimental set-up

Parameters	Values	Parameters for optimization algorithms	Values
VSI Power rating	10 kW	Population size (N_p)	50
AC Voltage	400 V	No. of iteration	100
rated AC Current	20 A	Inertia constant (w)	0.9
Input DC voltage (V_dc)	850 V	Acceleration constant ($c_1 = c_2$)	2
Inverter-side inductance (L_f)	2.53 mH	Distribution index for crossover (η_c)	20
Grid-side inductance (L_g)	2.53 mH	Distribution index for mutation (η_m)	20
Filter Capacitance (C_f)	10.03 μF	Crossover Probability (P_c)	0.8
Damping resistor (R_d)	1.588 Ω	Mutation Probability (P_m)	0.2
3Φ Inductive load	1 kVA, 0.9 pf	Lower bound (K_{Pmin}, K_{Imin})	1.5, 1500
Switching frequency (f_sw)	20 kHz	Upper bound (K_{pmax}, K_{Imax})	3, 3000
AC frequency (f_0)	50 Hz		
Sampling Time (T_s)	10 μs		
Cut-off frequency (ω_c)	31.41		
$P-f$ droop gain (m_p)	3.93e-4		
$Q-V$ droop gain (n_q)	4.08e-3		
Resistance line - 1 (R_{line1})	0.23 Ω		
Inductance line - 1 (L_{line1})	0.31 mH		
Resistance line - 2 (R_{line2})	0.35 Ω		
Inductance line - 2 (L_{line2})	1.85 mH		
Load - 1	7 kVA, 0.9 pf		
Load - 2	8 kVA, 0.9 pf		
Load - 3	20 kVA, 0.9 pf		

Table 5. Comparison of controller gain values and steady-state response with different controller tuning techniques.

Items	Gain values (K_p, K_I)	M_p	T_{ss} (sec)
ZN method	1.6821, 1587.06	12%	100
PSO	2.5, 2944.6	19%	89
Real coded based GA	2.2, 2316.3	15%	95

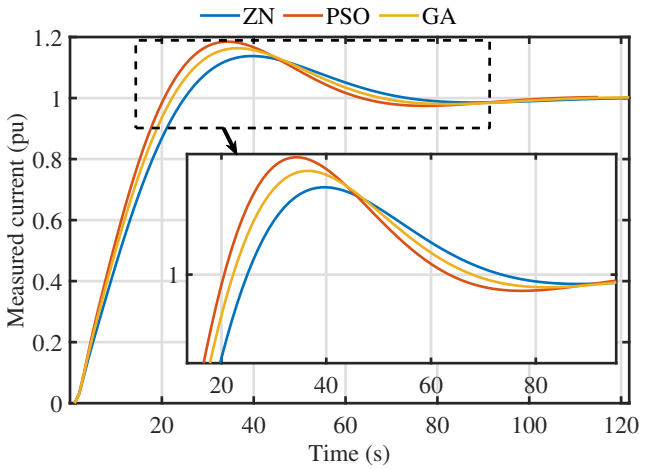

Figure 9. PI controller gain response comparison with ZN, PSO and GA

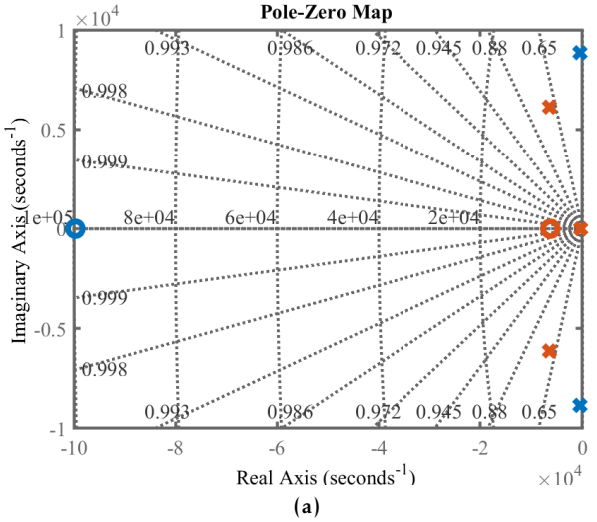

Figure 10. Stability analysis(a).Pole and zeros of the closed loop system with (red) and without (blue) damping, (b). Bode plot of the plant transfer function with(red) and without(blue) damping.

value and T_{ss} that aligns with the desired criteria. Consequently, the GA tuning method is selected for further experimental validation, as it meets all the specified criteria. The exploration into the controller's tracking performance under weak grid conditions is prompted by the intermittent nature of renewable sources and variations in load-side impedance. In this context, the figures, specifically fig. 12, 13, and 14, illustrate the dynamic response of the PI controller under various conditions during power regulation. These figures underscore the controller's efficacy in the nonlinear time domain, particularly when there are changes in output current from 15A to 20A, demonstrating its dynamic response and its capability to control reactive power effectively.

In fig. 11(a), we observe a voltage drop at the PCC as the distance between the main utility and the MG increases, as the system shown in fig. 1. This drop is significant, with PCC voltages (Vpeak value) decreasing from 280 V to 268.7 V to 260.3 V. When the power from the GFL decreases from 8 kW to 3 kW at t = 0.5 seconds, the stable PCC voltages are 260.7 V, 241.8 V, and 227.1 V, respectively. This voltage drop directly influences the Rate of Change of Frequency (ROCOF) or the nadir point, as shown in fig. 11(b). Increasing line length (L), with line resistance 0.436 ohm/km and inductance 0.987 mH/km (as per IEEE std. 1870-2019), leads to higher frequency dynamics and extended settling time, potentially causing a loss of synchronization with the utility. Also, the fig. 11 shows the weak grid impact on the voltage and frequency of the VSI.

Table 6 provides a detailed comparison of PCC voltage drops and nadir points in the frequency response for different grid SCRs.

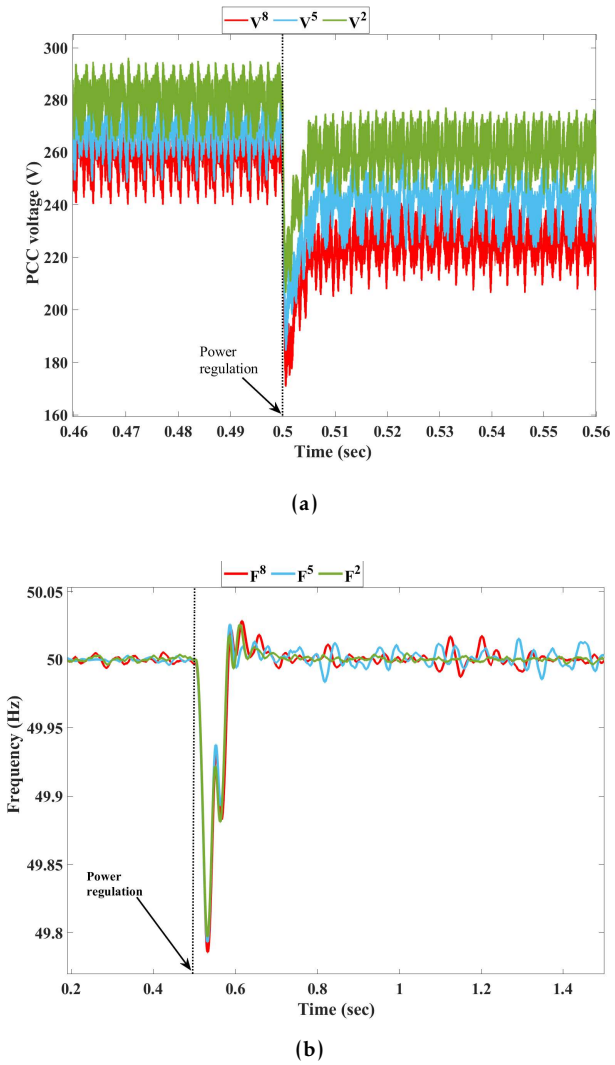

Figure 11. (a) Reference voltage (V_{ref}) comparison, (b) GFL frequency comparison with weak grid conditions.

Table 6. Comparison of different SCR ratings for a scenario with only GFL connected to the utility.

Parameters	L_1 = 2 km	L_2 = 5 km	L_3 = 8 km
Nadir points	49.80	49.79	49.78
PCC voltage (V)	260.7	241.8	227.1

Keeping a stable voltage at the PCC is crucial to ensure a reliable and high-quality power supply to customers. This improvement in the PCC voltage profile can also have a favorable impact on the Rate of Change of Frequency (ROCOF) during transient events within the distribution network, such as faults or sudden load changes. A stable voltage profile serves to mitigate the effects of these transients and strengthens the resilience of the network.

The experiment aims to verify the obtained controller parameters from real-coded based GA, see table 5, with the PI controllers' performance for weak grid operating conditions based on L_g variation and ($\frac{X}{R}$) variation, fault occurrence at the PCC and also tested for sudden load change in the standalone distributed network. The purpose of evaluating the stability and performance of the designed VSI components under dynamic operating conditions in standalone mode is to ensure that the system operates reliably and efficiently in real-world scenarios. This assessment helps identify any potential issues or limitations with the VSI components, such as voltage and current controllers, under varying load conditions, transient events, and disturbances. By conducting these evaluations, engineers can optimize the design parameters, improve system robustness, and mitigate risks associated with instability or performance degradation.

5.1. Parameter variation impact analysis

Effects due to L_g variations. In general, L_g is kept lower than L_f as suggested in many works of literature [45],[44]. Therefore, here the CCL performance is tested for the lower L_g values to achieve the considered objective for the designed filter. The controller performance is responsible for controlling the active and reactive power supply to the utility, as shown in fig. 12 (a) and (b). The figure implies that the controller achieves the steady state within the standard time (T_{ss} = 3 - 5 ms) and M_p within 5% for the CCL. We find the L_g variation for the transient condition in CCL, which could be responsible for the system's stability. The minimum L_g value has the maximum M_p and T_{ss}. The best controller tracking performance is obtained when L_g is set to 2.53 mH, the M_p and T_{ss} are within the desired criteria, see in fig. 12 (a). At this value, the inductance ratio (a_L) would be one, and the capacitor requires minimum energy storage, which also fulfills our filter design objective. From the above demonstration it is clear that as the controller performs worse as the L_g value decreases, so it is important to maintain the grid impedance according to the connection requirements. In weak grid scenarios, it is better to consider equalizing the value of L_f to reduce harmonics and current distortion at the load side.

Effect of ($\frac{X}{R}$) variations . To study dynamic conditions, two types of disturbances are considered; a sudden change in power demand and a change in the line impedance. In a low voltage distribution network, the lower line impedance at the grid side, in case of sudden load changes, creates a severe problem that affects the controller performance and overall system efficiency (especially lower SCR value systems due to over-current). In fig. 13 (a) and (b), the current is stepped up at 0.5 seconds to increase the power supply. The weak grid characteristics are defined as, SCR < 3 and $\frac{X}{R}$ < 5 [34]. Where The SCR specifies the maximum amount of power that the power system can handle

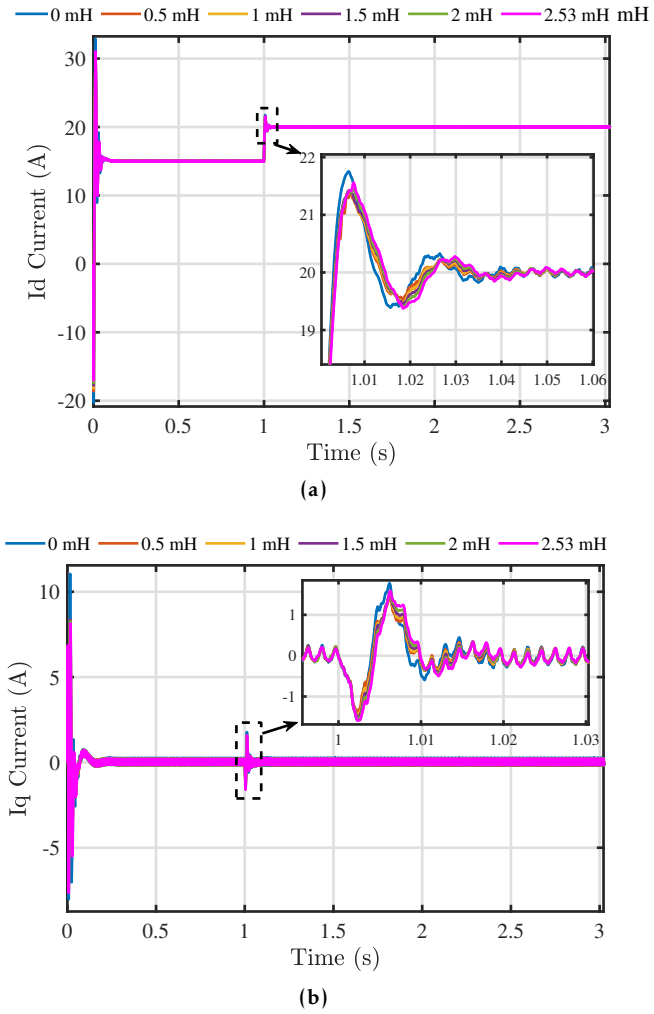

Figure 12. (a).Comparison of I_d current with L_g variation, (b). Comparison of I_q current with L_g variation.

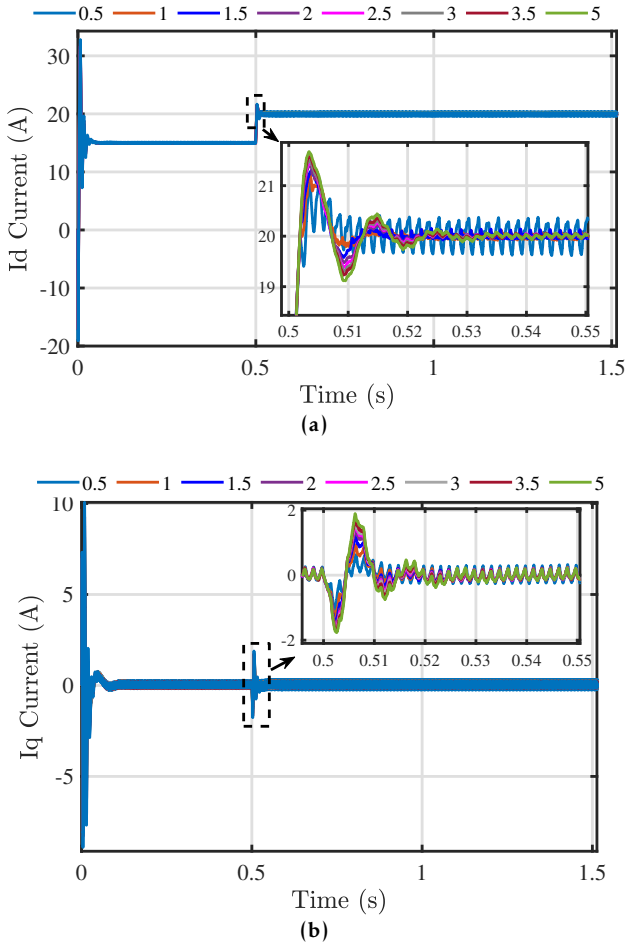

Figure 13. (a).Comparison of I_d current with $(\frac{X}{R})$ variations , (b). Comparison of I_q current with $(\frac{X}{R})$ variations.

without compromising power quality at the PCC. As shown in fig. 13 (a), the controller is quite robust to avoid the instability condition in the system and track the reference value with minimum oscillations.

Effect of fault occurrence at PCC. Generally, a three-phase fault is considered for the controller performance and the system withstands capacity for the short circuit current analysis during transient conditions. Because the maximum fault current occurs in 3-phase fault. When any fault occurs, the protection relay operating time is about 0.22 seconds [34]. The Critical Clearing Time (CCT) is a typical criterion for evaluating the transient stability limits. As we can see in fig. 14, the fault is cleared within CCT, and the current signal is back on the track set by the controller. The controller limits the fault current during the fault condition and does not allow it to exceed the desired value. It shows the robustness of the controller and fault ride-through capability for lower strength systems to recover the voltage stability after the fault.

5.2. THD analysis

PI controller operates on a fixed frequency of the system, so its output could be unstable under weak grid conditions. The output current THD levels are below 3% as per requirements for the weak grid applications, which shows the quality of the output current shown in fig. 15(a). THD levels in the output voltages of multiple DG units during a sudden load change while operating in an IS mode, which are quite satisfactory, and they meet the stringent standards established by IEEE std. 519, as shown in fig. 15(b).

5.3. Controller performance analysis in Standalone mode

In fig. 8, the designed three VSIs (10kVA each) are connected to a distributed network in standalone mode for testing the stability and reliability performance.

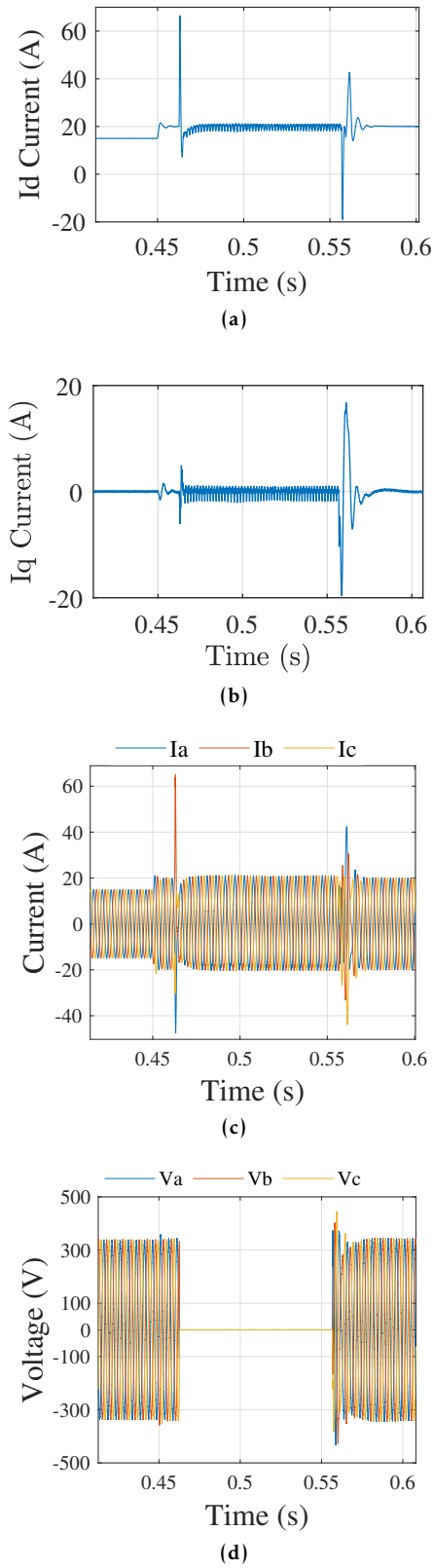

Figure 14. (a). I_d current , (b). I_q current , (c). VSI output 3ϕ - current during the fault condition , (d). Output 3ϕ - voltage during the fault condition .

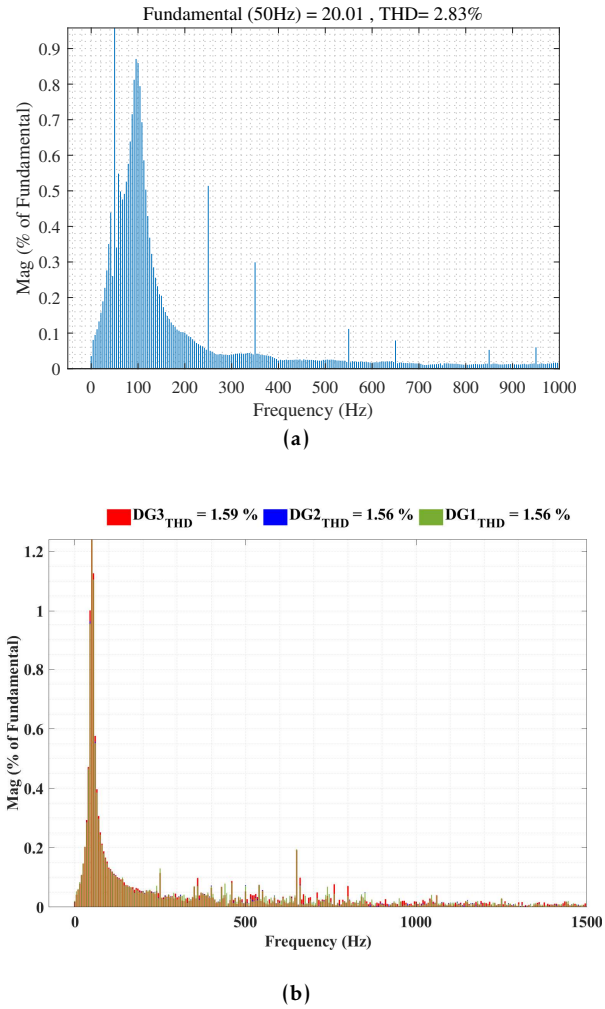

Figure 15. THD analysis of VSI output current(a).for PI controller, (b). THD analysis of DG units (shown in fig. 7) during a sudden load change in IS mode.

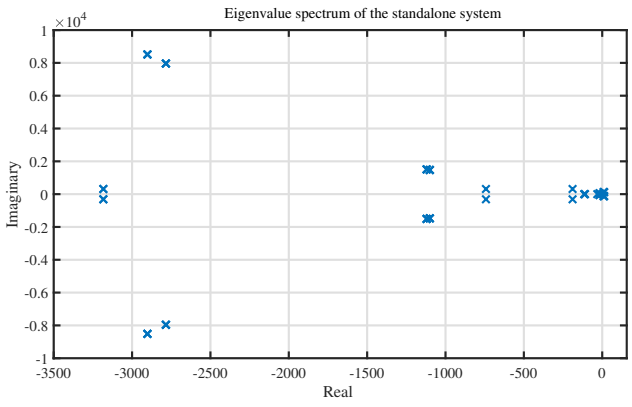

Figure 16. Eigenvalue spectrum of three VSI in standalone mode

The eigenvalue spectrum of the consider network in fig. 16 demonstrates the effectiveness of the designed controller system. The negative eigenvalues indicate

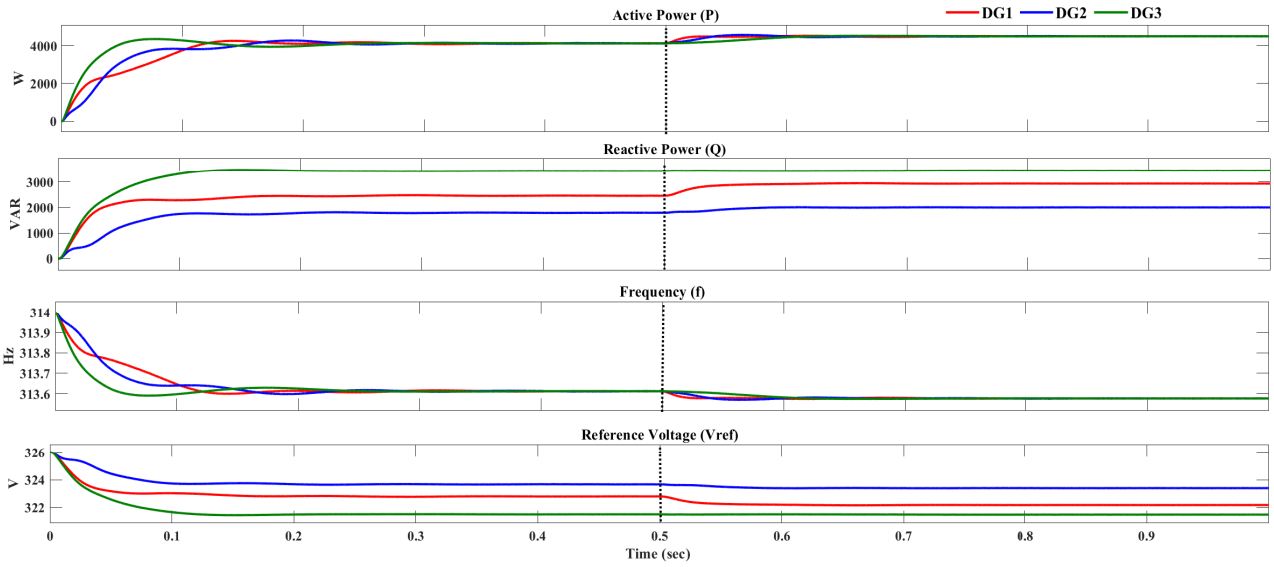

Figure 17. Stability analysis of the three VSI standalone system when sudden load increased at 0.5 sec

that the system remains stable during standalone operation. The different cluster positions show the different modes in the microgrid system, such as distribution line, filter, power, voltage, and current controller state variables. Fig. 17 and 18 demonstrates the effectiveness of the controller tracking performance when there is a sudden 20% increase in load-1 at DG-1. The small load variation at a particular DG in the network, while here the load increase occurs at 0.5 seconds, leading to changes in active power sharing and consequently affecting the VSI frequency shown in the figure. However, active power oscillations may occur between parallel inverters during the load fluctuations, but here the power flow is smooth without using any external damping techniques.

5.4. Controller performance validation

The plant function, considering all aspects outlined in section III, and tested it in MATLAB/SIMULINK. This testing helps us select accurate parameters in line with standard requirements [4], [9]. The controller gain values have been diligently calculated using three distinct methods to optimize controller performance during operation. These optimization algorithms have been implemented in custom m-files. The effectiveness of the controller loop optimization has been rigorously tested and verified using the Typhoon real-time emulator model-604, which provides an impressive 20-nsec sampling resolution. In fig. 19(a), the schematic editor is used for VSI modeling purposes, which is compiled with the real-time hardware emulator set-up, and the SCADA (Supervisory Control And Data Acquisition) panel is used for monitoring and visualization of the output results. The Typhoon set-up is connected through the Ethernet connection mode to the desktop system. The validation on Hardware-In-Loop implementation is completely reliable for the coordinated power feeding to the utility from different power generation sources through the connected power converter as shown in fig. 19(b).

5.5. Discussion

According to the findings in [9], the parameter optimization has yielded satisfactory results, as the THD level of the VSI output current remains consistently below 3%. In direct comparison to the results presented in [14], it is evident that the filter and controller parameters, as well as the resulting THD levels, are improved and better than the given results in the mentioned paper for the same inverter rating. Moreover, weak grid stability issues discussed in references such as [36] and [54] have been successfully addressed through the application of universal control modeling and various operating conditions tailored to weak grid scenarios. To mitigate the impact of grid- side impedance variations on CCL, this study has systematically tested different controller tuning methods, meticulously documented in table 5. The stability of the impedance variation-based controller performance is demonstrated in fig. 12 and 13. The study's rigor extends to testing the VSI's performance during different scenarios to demonstrate the robustness of the designed filter and controller parameters affect. The results collectively demonstrate that the designed VSI parameters are versatile and capable at handling a spectrum of scenarios, particularly in less stable conditions. We can see the performance of the single loop control based VSI controller operation

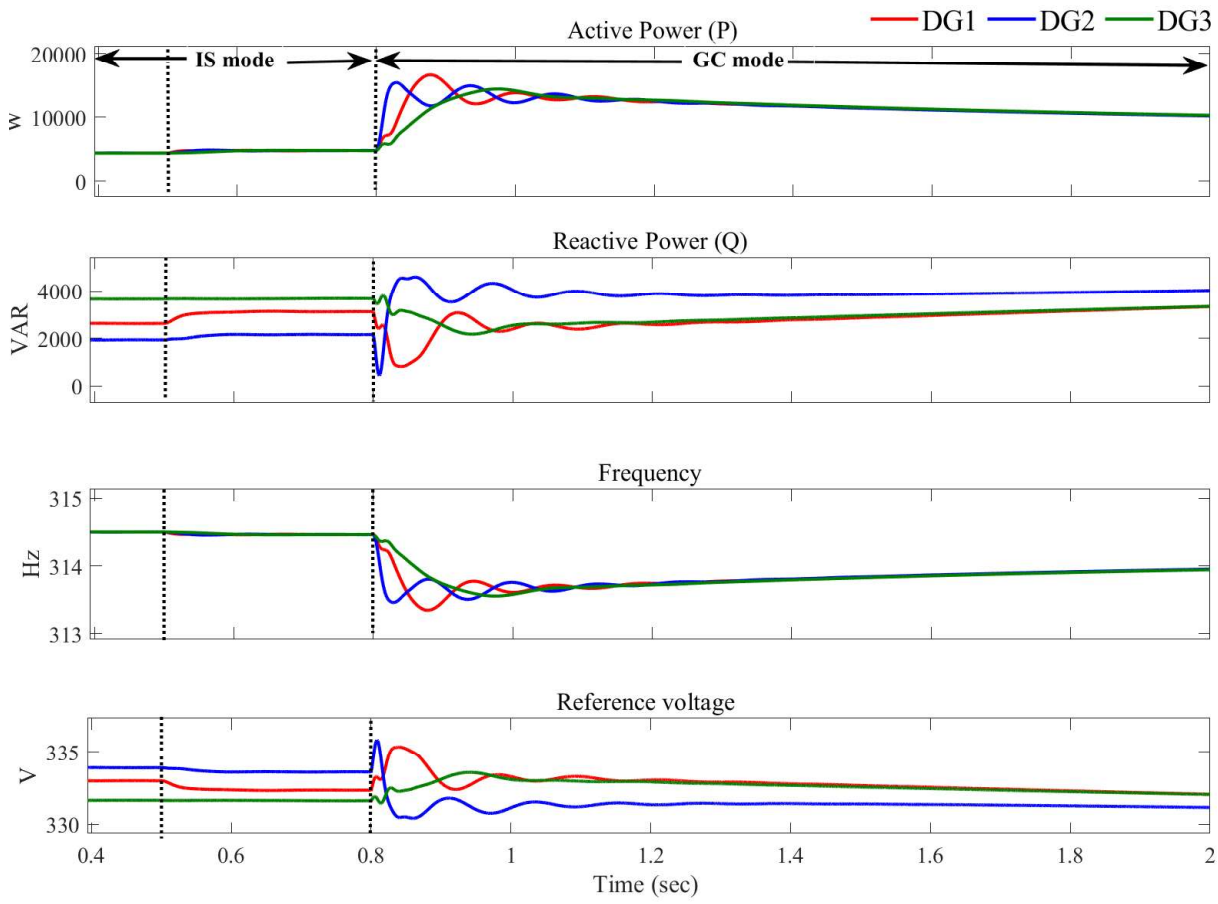

Figure 18. MG transition from IS mode to GC mode, where load switching occurs at t = 0.5 sec and mode switching at t = 0.8 sec.

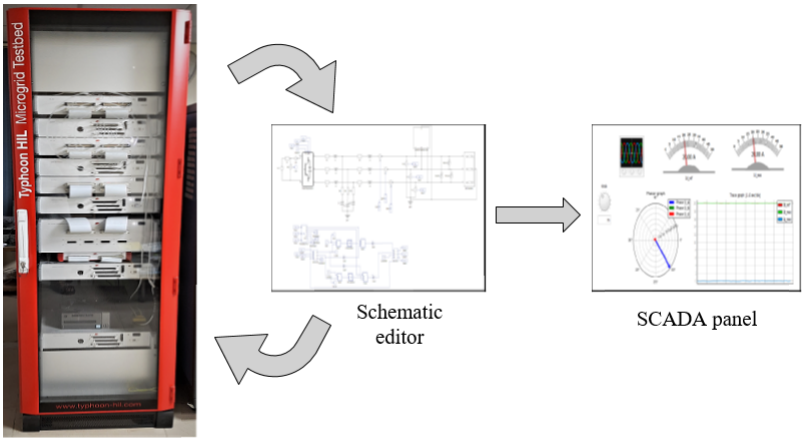

Figure 19. Experimental set-up: Typhoon-Hil emulator 604 set-up in real-time mode.

with L_g variation, $\frac{X}{R}$ variation and fault analysis. In weak grid condition the interaction between PLL and CCL can introduce current distortion. Therefore, the Comprehensive CCL tracking performance underscores the VSI's reliability even in challenging real-time conditions. The same VSI is used with DG units as given in fig. 8, to investigate the performance and stability analysis in MG. Fig. 18 shows the stable MG operation

of the DG units in different operating modes which are similar as real real world conditions.

6. Conclusion and Future Scope

In this paper, the grid impedance-based stability is concerned and improves the inverter stability for lower-voltage distribution networks. There has been many research done on the inverters controlling and stability issues related to different scenarios. But to get the improvements and resolve many other related problems, we try to design and calculate the inverter parameters as per the considered objectives. Here, we have investigated the medium-level (rating 10 kW) inverter operation in different MG operating conditions to improve consumer-side stability and power quality issues. Finally, it investigates the designed system parameters for controller tracking performance, while variations in L_g and $\frac{X}{R}$ show the impact on controller performance during grid-side impedance variations. The controller tracking performance is satisfactory for the weak grid impedance scenarios. Performance in fault occurrence and sudden load change conditions shows the robustness of the system. The results could be used to develop synchronization control strategies and design features to improve the resilience and stability of MGs. The results obtained show stable MG operation in both modes and grid stability after connection. The THD level represents the power quality of the MG in both modes of operation.

For further research in the field of MG stability under weak grid conditions, integrating virtual impedance at the output of power converters can improve overall system stability. Key avenues for exploration include investigating the frequency stability and ROCOF of VSIs for grid synchronization, along with effective reactive power sharing management at the PCC. Additionally, implementing a Virtual Synchronous Generator (VSG) with a GFM inverter can be highly beneficial in low-inertia environments. Since GFL inverters often struggle with stability and dynamic performance under weak grid conditions, a combined operation of GFM and GFL inverters can help maintain both voltage and frequency stability in such scenarios.

References

[1] Panigrahi, R., Mishra, S. K., Srivastava, S. C., Srivastava, A. K., & Schulz, N. N. (2020). Grid integration of small-scale photovoltaic systems in secondary distribution network—A review. IEEE Transactions on Industry Applications, 56(3), 3178-3195.

[2] Figueira, H. H., Hey, H. L., Schuch, L., Rech, C., & Michels, L. (2015, June). Brazilian grid-connected photovoltaic inverters standards: A comparison with IEC and IEEE. In 2015 IEEE 24th International Symposium on Industrial Electronics (ISIE) (pp. 1104-1109). IEEE.

[3] Wu, Y. K., Lin, J. H., & Lin, H. J. (2017). Standards and guidelines for grid-connected photovoltaic generation systems: A review and comparison. IEEE Transactions on Industry Applications, 53(4), 3205-3216.

[4] IEEE Standards Board. (2003). IEEE Standard for Interconnecting Distributed Resources with Electric Power Systems: 1547-2003. IEEE.

[5] Standard, I. E. C. (2004). Photovoltaic (pv) systems-characteristics of the utility interface. IEC: Geneva, Switzerland.

[6] IEEE Recommended Practice for Utility Interface of Photovoltaic (PV) Systems,(2000), in IEEE Std 929-2000, doi: 10.1109/IEEESTD.2000.91304.

[7] VDE (2012). VDE-AR-N 4105:2011-08 Power generation systems connected to the low-voltage distribution network.

[8] California Public Utilities Commission. (2014). Rule 21 Generating Facility Interconnections. California Public Utilities Commission: San Francisco, CA, USA.

[9] Blooming, T. M., & Carnovale, D. J. (2006, June). Application of IEEE Std 519-1992 harmonic limits. In Conference Record of 2006 Annual Pulp and Paper Industry Technical Conference (pp. 1-9). IEEE.

[10] IEEE Standard for Harmonic Control in Electric Power Systems, (2022), in IEEE Std 519-2022 (Revision of IEEE Std 519-2014) , pp.1-31, 5 Aug. 2022, doi: 10.1109/IEEESTD.2022.9848440.

[11] IEEE Recommended Practice and Requirements for Harmonic Control in Electric Power Systems, (2014) in IEEE Std 519-2014 (Revision of IEEE Std 519-1992), pp.1-29, 11 June 2014, doi: 10.1109/IEEESTD.2014.6826459.

[12] Channegowda, P., & John, V. (2010). Filter optimization for grid interactive voltage source inverters. IEEE Transactions on Industrial Electronics, 57(12), 4106-4114.

[13] Prodanovic, M., & Green, T. C. (2003). Control and filter design of three-phase inverters for high power quality grid connection. IEEE transactions on Power Electronics, 18(1), 373-380.

[14] Isen, E., & Bakan, A. F. (2016). Development of 10 kW three-phase grid connected inverter. automatika, 57(2), 319-328.

[15] Rocabert, J., Luna, A., Blaabjerg, F., & Rodriguez, P. (2012). Control of power converters in AC microgrids. IEEE transactions on power electronics, 27(11), 4734-4749.

[16] Holmes, D. G., Lipo, T. A., Mcgrath, B. P., & Kong, W. Y. (2009). Optimized design of stationary frame three phase AC current regulators. IEEE transactions on power electronics, 24(11), 2417-2426.

[17] Timbus, A., Liserre, M., Teodorescu, R., Rodriguez, P., & Blaabjerg, F. (2009). Evaluation of current controllers for distributed power generation systems. IEEE Transactions on power electronics, 24(3), 654-664.

[18] Basilio, J. C., & Matos, S. R. (2002). Design of PI and PID controllers with transient performance specification. IEEE Transactions on education, 45(4), 364-370.

[19] Rivera, D. E., Morari, M., & Skogestad, S. (1986). Internal model control: PID controller design. Industrial & engineering chemistry process design and development, 25(1), 252-265.

[20] Hassan, M. A., & Abido, M. A. (2010). Optimal design of microgrids in autonomous and grid-connected modes using particle swarm optimization. IEEE Transactions on power electronics, 26(3), 755-769.
[21] Hu, J., Zhu, J., & Dorrell, D. G. (2014). Model predictive control of grid-connected inverters for PV systems with flexible power regulation and switching frequency reduction. IEEE Transactions on Industry Applications, 51(1), 587-594.
[22] Temiz, H., Keysan, O., & Demirok, E. (2020). Adaptive controller based on grid impedance estimation for stable operation of grid-connected inverters under weak grid conditions. IET Power Electronics, 13(13), 2692-2705.
[23] IEEE Guide for Planning DC Links Terminating at AC Locations Having Low Short-Circuit Capacities, (1917) in IEEE Std 1204-1997,1-216, 21 Jan. 1997, doi: 10.1109/IEEESTD.1997.85949.
[24] Del Valle, Y., Venayagamoorthy, G. K., Mohagheghi, S., Hernandez, J. C., & Harley, R. G. (2008). Particle swarm optimization: basic concepts, variants and applications in power systems. IEEE Transactions on evolutionary computation, 12(2), 171-195.
[25] Kennedy, J., & Eberhart, R. (1995, November). Particle swarm optimization. In Proceedings of ICNN'95-international conference on neural networks (Vol. 4, pp. 1942-1948).
[26] Deb, K., Sindhya, K., & Okabe, T. (2007, July). Self-adaptive simulated binary crossover for real-parameter optimization. In Proceedings of the 9th annual conference on genetic and evolutionary computation (pp. 1187-1194).
[27] Awouda, A. E. A., & Mamat, R. B. (2010, February). Refine PID tuning rule using ITAE criteria. In 2010 The 2nd International conference on computer and automation engineering (ICCAE) (Vol. 5, pp. 171-176). IEEE.
[28] Rodríguez-Molina, A., Mezura-Montes, E., Villarreal-Cervantes, M. G., & Aldape-Pérez, M. (2020). Multi-objective meta-heuristic optimization in intelligent control: A survey on the controller tuning problem. Applied Soft Computing, 93, 106342.
[29] Osório, C. R., Borin, L. C., Koch, G. G., & Montagner, V. F. (2019, December). Optimization of robust PI controllers for grid-tied inverters. In 2019 IEEE 15th Brazilian Power Electronics Conference and 5th IEEE Southern Power Electronics Conference (COBEP/SPEC) (pp. 1-6). IEEE.
[30] Oliveira, A. C., Jacobina, C. B., & Lima, A. M. N. (2007). Improved dead-time compensation for sinusoidal PWM inverters operating at high switching frequencies. IEEE Transactions on Industrial Electronics, 54(4), 2295-2304.
[31] Liu, Y., Ben, H., Li, C., & Wang, D. (2012, June). Research of the dead-time compensation based on the three-phase grid-connected inverter. In Proceedings of The 7th International Power Electronics and Motion Control Conference (Vol. 1, pp. 510-514). IEEE.
[32] Alenius, H., Berg, M., Luhtala, R., & Roinila, T. (2019, October). Stability and performance analysis of grid-connected inverter based on online measurements of current controller loop. In IECON 2019-45th Annual Conference of the IEEE Industrial Electronics Society (Vol. 1, pp. 2013-2019). IEEE.
[33] Pattabiraman, D., Lasseter, R. H., & Jahns, T. M. (2018, August). Comparison of grid following and grid forming control for a high inverter penetration power system. In 2018 IEEE Power & Energy Society General Meeting (PESGM) (pp. 1-5). IEEE.
[34] Jayasinghe, G., & Bahrani, B. (2021, June). Stability-Enhancing Measures for Weak Grids Study Australian Renewable Energy Agency, Milestone2 report.
[35] Meersman, B., Renders, B., Degroote, L., Vandoorn, T., & Vandevelde, L. (2010, July). The influence of grid-connected three-phase inverters on voltage unbalance. In IEEE PES General Meeting (pp. 1-9). IEEE.
[36] Zhang, Q., Mao, M., Ke, G., Zhou, L., & Xie, B. (2020). Stability problems of PV inverter in weak grid: a review. IET Power Electronics, 13(11), 2165-2174.
[37] Saïd-Romdhane, M. B., Naouar, M. W., Slama-Belkhodja, I., & Monmasson, E. (2016). Robust active damping methods for LCL filter-based grid-connected converters. IEEE transactions on power electronics, 32(9), 6739-6750.
[38] Hu, X., Liu, T., He, C., Ma, Y., Su, Y., Yin, H., & Liu, Y. (2020). Real-time power management technique for microgrid with flexible boundaries. IET Generation, Transmission & Distribution, 14(16), 3161-3170.
[39] Moretti, L., Meraldi, L., Niccolai, A., Manzolini, G., & Leva, S. (2021). An innovative tunable rule-based strategy for the predictive management of hybrid microgrids. Electronics, 10(10), 1162.
[40] Rakhshani, E., Rouzbehi, K., Elsaharty, M. A., & Cortes, P. R. (2017). Heuristic optimization of supplementary controller for VSC-HVDC/AC interconnected grids considering PLL. Electric Power Components and Systems, 45(3), 288-301.
[41] Teodorescu, R., Blaabjerg, F., Liserre, M., & Loh, P. C. (2006). Proportional-resonant controllers and filters for grid-connected voltage-source converters. IEE Proceedings-Electric Power Applications, 153(5), 750-762.
[42] Jalili, K., & Bernet, S. (2009). Design of *LCL* filters of active-front-end two-level voltage-source converters. IEEE Transactions on Industrial Electronics, 56(5), 1674-1689.
[43] Liserre, M., Blaabjerg, F., & Hansen, S. (2005). Design and control of an LCL-filter-based three-phase active rectifier. IEEE Transactions on industry applications, 41(5), 1281-1291.
[44] Bernet, S., Ponnaluri, S., & Teichmann, R. (2002). Design and loss comparison of matrix converters, and voltage-source converters for modern AC drives. IEEE Transactions on Industrial Electronics, 49(2), 304-314.
[45] Han, Y., Yang, M., Li, H., Yang, P., Xu, L., Coelho, E. A. A., & Guerrero, J. M. (2019). Modeling and stability analysis of *LCL*-type grid-connected inverters: A comprehensive overview. IEEE Access, 7, 114975-115001.
[46] Karshenas, H. R., & Saghafi, H. (2006, July). Basic criteria in designing LCL filters for grid connected converters. In 2006 IEEE International Symposium on Industrial Electronics (Vol. 3, pp. 1996-2000). IEEE.
[47] Wang, T. C., Ye, Z., Sinha, G., & Yuan, X. (2003, June). Output filter design for a grid-interconnected three-phase inverter. In IEEE 34th Annual Conference on Power

Electronics Specialist, 2003. PESC'03. (Vol. 2, pp. 779-784). IEEE.
[48] Zou, Z., Wang, Z., & Cheng, M. (2013). Modeling, analysis, and design of multifunction grid-interfaced inverters with output LCL filter. IEEE Transactions on Power Electronics, 29(7), 3830-3839.
[49] He, J., & Li, Y. W. (2011). Generalized closed-loop control schemes with embedded virtual impedances for voltage source converters with LC or LCL filters. IEEE Transactions on Power Electronics, 27(4), 1850-1861.
[50] Domański, P. D. (2020). Control Performance Assessment: Theoretical Analyses and Industrial Practice (Vol. 245). Cham: Springer.
[51] Singh, H. P., Swami, A. K. (2019). A Review of Power Quality Improvements by using FACTS devices. International Journal of Engineering and Science (IJES), 8, 53-64.
[52] Parvez, M., Elias, M. F. M., Abd Rahim, N., Blaabjerg, F., Abbott, D., & Al-Sarawi, S. F. (2020). Comparative study of discrete PI and PR controls for single-phase UPS inverter. IEEE Access, 8, 45584-45595.
[53] Pogaku, N., Prodanovic, M., & Green, T. C. (2007). Modeling, analysis and testing of autonomous operation of an inverter-based microgrid. IEEE Transactions on power electronics, 22(2), 613-625.
[54] Peng, Q., Jiang, Q., Yang, Y., Liu, T., Wang, H., & Blaabjerg, F. (2019). On the stability of power electronics-dominated systems: Challenges and potential solutions. IEEE Transactions on Industry Applications, 55(6), 7657-7670.
[55] H. P. Singh, A. Sharma, S. Bose and A. K. Swami, (2024) State space modelling and seamless transition between Islanded and Grid-connected operation modes, International Conference on Intelligent and Innovative Technologies in Computing, Electrical and Electronics (IITCEE), Bangalore, India, pp. 1-6, doi: 10.1109/IITCEE59897.2024.10467393.
[56] Kumar, S., & Singh, B. (2018). Seamless operation and control of single-phase hybrid PV-BES-utility synchronized system. IEEE Transactions on Industry Applications, 55(2), 1072-1082.
[57] Rosso, R., Wang, X., Liserre, M., Lu, X., & Engelken, S. (2021). Grid-forming converters: Control approaches, grid-synchronization, and future trends—A review. IEEE Open Journal of Industry Applications, 2, 93-109.
[58] Liu, T., Wang, X., Liu, F., Xin, K., & Liu, Y. (2022). Transient stability analysis for grid-forming inverters transitioning from islanded to grid-connected mode. IEEE Open Journal of Power Electronics, 3, 419-432.
[59] Li, C., Yang, Y., Cao, Y., Wang, L., & Blaabjerg, F. (2020). Frequency and voltage stability analysis of grid-forming virtual synchronous generator attached to weak grid. IEEE Journal of Emerging and Selected Topics in Power Electronics, 10(3), 2662-2671.
[60] Wang, J., Pratt, A., & Baggu, M. (2019, August). Integrated synchronization control of grid-forming inverters for smooth microgrid transition. In 2019 IEEE Power & Energy Society General Meeting (PESGM) (pp. 1-5). IEEE.
[61] Li, Y., Gu, Y., & Green, T. C. (2022). Revisiting grid-forming and grid-following inverters: A duality theory. IEEE Transactions on Power Systems, 37(6), 4541-4554.
[62] Alghamdi, B., & Cañizares, C. A. (2020). Frequency regulation in isolated microgrids through optimal droop gain and voltage control. IEEE Transactions on Smart Grid, 12(2), 988-998.
[63] H. P. Singh, S. Som, A. Sharma, S. Bose and A. K. Swami, (2023) Seamless transition of inverters from islanding to grid-connected mode connected to weak grid, IEEE 2nd Industrial Electronics Society Annual On-Line Conference (ONCON), SC, USA, pp. 1-6, doi: 10.1109/ONCON60463.2023.10431030.
[64] Du, W., Chen, Z., Schneider, K. P., Lasseter, R. H., Nandanoori, S. P., Tuffner, F. K., & Kundu, S. (2019). A comparative study of two widely used grid-forming droop controls on microgrid small-signal stability. IEEE Journal of Emerging and Selected Topics in Power Electronics, 8(2), 963-975.
[65] Amin, M., & Zhong, Q. C. (2019). Resynchronization of distributed generation based on the universal droop controller for seamless transfer between operation modes. IEEE Transactions on Industrial Electronics, 67(9), 7574-7582.
[66] IEEE Standard for the Specification of Microgrid Controllers, in IEEE Std 2030.7-2017, pp.1-43, 23 April 2018, doi: 10.1109/IEEESTD.2018.8340204.